The Effects of Divergent and Nondivergent Winds on the Kinetic Energy Budget of a Mid-Latitude Cyclone: A Case Study

TSING-CHANG CHEN

Department of Meteorology, Massachusetts Institute of Technology, Cambridge 02139

JORDAN C. ALPERT

Department of Atmospheric and Oceanic Science, University of Michigan, Ann Arbor 48104

THOMAS W. SCHLATTER

National Center for Atmospheric Research,[1] Boulder, Colo. 80307

(Manuscript received 1 November 1977, in final form 5 January 1978)

ABSTRACT

The magnitude of the divergent component of the wind is relatively small compared to that of the nondivergent component in large-scale atmospheric flows; nevertheless, it plays an important role in the case of explosive cyclogenesis examined here. We have calculated the kinetic energy budget for the life cycle of an intense, developing cyclone over North America. The principal kinetic energy source is the net horizontal transport across the boundaries of the region enclosing the cyclone. By investigating the relative importance of the divergent and nondivergent wind components in the kinetic energy budget, we found, as expected, that neglecting the divergent wind component in calculating the magnitude of the kinetic energy is of little consequence, but that the horizontal flux convergence and generation of kinetic energy depend crucially upon the divergent component. Modification of the divergent wind component can result in significant changes in the kinetic energy budget of the synoptic system.

1. Introduction

The earliest numerical weather prediction experiments were conducted by Charney *et al.* (1950) at Princeton. Their initial success with a barotropic model prompted development of more complicated quasi-geostrophic models capable of filtering gravity waves and simulating the development of weather systems. Following rapid advances in computing technology in the late fifties, meteorologists returned to Richardson's (1922) early attempt to use the primitive equations as the basis for prediction models. It is well known that the primitive equations contain slow-moving meteorologically important waves as well as high-speed gravity waves. The latter are excited by horizontal divergence in the initial data and can be amplified, eventually spoiling the numerical prediction. The lack of suitable treatment of initial data was one reason for Richardson's failure (Thompson, 1961). When the primitive equation prediction model was first applied some two decades ago, Charney (1955) reduced horizontal divergence in the initial data by means of a nonlinear balance equation. Since then, meteorologists have developed more sophisticated schemes for controlling divergence and balancing the large-scale wind and pressure fields [see, e.g., Washington and Baumhefner (1975) and the review by Haltiner (1971)].

Although the divergent component of the wind is small, it is premature to say that it should be removed from initial wind fields for numerical prediction models. Chen and Wiin-Nielsen (1976) showed that the divergent wind may play an important role in global atmospheric energetics. In this paper we examine the relative contributions of the divergent and nondivergent wind components to the kinetic energy budget of a developing cyclone.

In the following sections, we discuss the kinetic energy equations, the data sources and method of analysis, the synoptic situation, the kinetic energy budget and, finally, the importance of including the divergent wind component in the initial state.

2. Kinetic energy equation

In pressure coordinates, the rate of change of kinetic energy in an atmospheric column is

$$\frac{\partial K}{\partial t} \equiv \frac{1}{sg}\int_0^{P_0}\int_s \frac{\partial k}{\partial t}\,ds\,dp = -\frac{1}{sg}\int_0^{P_0}\int_s \nabla\cdot(\mathbf{V}k)\,ds\,dp - \frac{1}{sg}\int_0^{P_0}\int_s \frac{\partial}{\partial p}(\omega k)\,ds\,dp$$

[1] The National Center for Atmospheric Research is sponsored by the National Science Foundation.

0027-0644/78/0458-0468$05.50

$$-\frac{1}{sg}\int_0^{P_0}\int_s \mathbf{V}\cdot\nabla\phi\,ds\,dp - D(k), \quad (1)$$

where s is the area of computational domain, g the acceleration due to gravity, P_0 the surface pressure, and $D(k)$ the dissipation of kinetic energy. On the right-hand side of (1), the first and second terms are the horizontal and vertical flux divergence of kinetic energy, respectively; the third term is the generation of kinetic energy due to the cross-contour flow. Energy variables designated by capital letters, e.g., K, K_R and K_D are vertically integrated and area-averaged.

According to Helmholtz's theorem, the total wind is the sum of the divergent wind V_D and the nondivergent (or rotational) wind $\mathbf{V}_R$, i.e.,

$$\mathbf{V}=\mathbf{V}_R+\mathbf{V}_D. \quad (2)$$

The kinetic energy per unit mass can be expressed as

$$k\equiv\tfrac{1}{2}\mathbf{V}\cdot\mathbf{V}=k_R+k_D+\mathbf{V}_R\cdot\mathbf{V}_D, \quad (3)$$

where

$$k_R=\tfrac{1}{2}\mathbf{V}_R\cdot\mathbf{V}_R \quad \text{and} \quad k_D=\tfrac{1}{2}\mathbf{V}_D\cdot\mathbf{V}_D. \quad (4)$$

Using (2), we may write the integrands of the first and third terms on the right-hand side of (1) as

$$-\nabla\cdot(\mathbf{V}k)=-\nabla\cdot(\mathbf{V}_Rk)-\nabla\cdot(\mathbf{V}_Dk), \quad (5)$$

$$-\mathbf{V}\cdot\nabla\phi=-\mathbf{V}_R\cdot\nabla\phi-\mathbf{V}_D\cdot\nabla\phi. \quad (6)$$

Eq. (5) shows that the horizontal flux convergence of kinetic energy is caused by the horizontal transport of nondivergent and divergent winds. For convenience we associate $-\mathbf{V}_R\cdot\nabla\phi$ and $-\mathbf{V}_D\cdot\nabla\phi$ with the generation of kinetic energy due to barotropic and baroclinic processes, respectively (Pearce, 1974; Chen and Wiin-Nielsen, 1976). The barotropic term integrates to zero in a closed domain (Chen and Wiin-Nielsen, 1976), but not in an open domain as considered here. Using (5) and (6), we can rewrite (1) as

$$\frac{1}{sg}\int_0^{P_0}\int_s\frac{\partial k}{\partial t}ds\,dp=-\frac{1}{sg}\int_0^{P_0}\int_s\nabla\cdot(\mathbf{V}_Rk)ds\,dp$$
$$-\frac{1}{sg}\int_0^{P_0}\int_s\nabla\cdot(\mathbf{V}_Dk)ds\,dp$$
$$-\frac{1}{sg}\int_0^{P_0}\int_s\frac{\partial}{\partial p}(\omega k)ds\,dp-\frac{1}{sg}\int_0^{P_0}\int_s\mathbf{V}_R\cdot\nabla\phi\,ds\,dp$$
$$-\frac{1}{sg}\int_0^{P_0}\int_s\mathbf{V}_D\cdot\nabla\phi\,ds\,dp-D(k). \quad (7)$$

We shall pay particular attention to the contribution of $\mathbf{V}_R$ and $\mathbf{V}_D$ to k in (3), to the horizontal flux convergence of kinetic energy $-\nabla\cdot(\mathbf{V}k)$ in (5), and to the generation of kinetic energy $-\mathbf{V}\cdot\nabla\phi$ in (6). If we neglect the divergent wind, then (7) becomes

$$\frac{1}{sg}\int_0^{P_0}\int_s\frac{\partial k}{\partial t}ds\,dp=-\frac{1}{sg}\int_0^{P_0}\int_s\nabla\cdot(\mathbf{V}_Rk)ds\,dp$$
$$-\frac{1}{sg}\int_0^{P_0}\int_s\frac{\partial}{\partial p}(\omega k)ds\,dp$$
$$-\frac{1}{sg}\int_0^{P_0}\int_s\mathbf{V}_R\cdot\nabla\phi\,ds\,dp-D(k). \quad (8)$$

By evaluating (8), we show how neglect of the divergent wind affects the kinetic energy budget of a developing cyclone.

3. Data and computations

The data for this study are 12 h, North American rawinsonde winds and heights on mandatory pressure surfaces and surface synoptic reports from 1200 GMT 12 March through 1200 GMT 16 March 1973. Sea level pressure and upper air winds and heights at 850, 700, 500, 400, 300, 250, 200 and 150 mb were estimated on a 2.5° latitude-longitude grid with the limited-area version of a multivariate statistical objective analysis scheme described by Schlatter (1975) and Schlatter *et al.* (1976). In this scheme, patterned after Gandin's (1963) "optimal interpolation" method, the analysis of the wind field depends on both wind and height observations. The analyzed winds yield divergence values of 10^{-5} to 10^{-6} s^{-1}, typical of synoptic-scale disturbances (Haltiner and Martin, 1957), a fact crucial to the present study. The objective analysis domain extends from 7.5° to 75°N and from 150° to 50°W. Protected from boundary effects in the analysis scheme by a "buffer" zone of at least 20° in latitude and longitude is an inner domain used for kinetic energy budget calculations. It extends from 27.5° to 52.5°N and from 122.5° to 75.0°W (Fig. 1) and includes the cyclone within its boundaries during growth and decay.

The horizontal wind vector is separated into its divergent and nondivergent components by means of an iterative method (Endlich, 1967) that we will describe briefly here. First, the vorticity is calculated from the analyzed wind by means of centered differences. Let a grid point's nearest neighbors to the east, west, north and south be designated by e, w, n and s, respectively. Adjustments of equal magnitude but opposite sign are then made to u_e, and u_w and likewise to v_n and v_s, so that the divergence at the central grid point vanishes. After application of this procedure at every point on the grid, the vorticity of the adjusted wind field is different from that of the analyzed wind field; but a second round of adjustments involving u_n, u_s, v_e and v_w at each grid point can bring them into closer agreement. With repeated applications of the

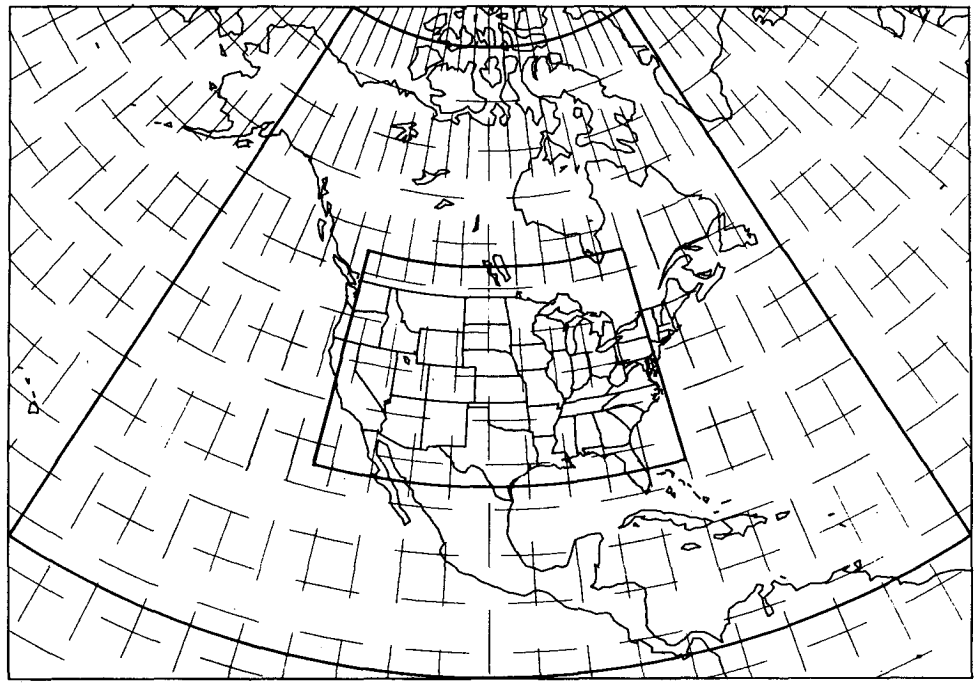

FIG. 1. Wind analyses are performed in the larger region indicated on this map. The kinetic energy budget is calculated within the inner region.

algorithm just described, the divergence of the adjusted wind approaches zero and its vorticity approaches that of the analyzed wind.

A constant correction is added to the u and v components of the final adjusted wind so that the average values of the nondivergent components agree with the average values of the analyzed components. The divergent wind is calculated as the vector difference between the analyzed wind and the nondivergent wind.

The vertical velocity fields are calculated by the kinematic method, that is, by vertical integration of the continuity equation. The adjustment scheme suggested by O'Brien (1970) is applied, with the vertical velocity assumed to be zero at 1000 mb and at the top of the atmosphere.

The energy variables are calculated at 0000 and 1200 GMT. Therefore, time derivatives evaluated by central differences spanning 24 h may be too small, but they give a reasonable indication of the time variation of kinetic energy. For lack of wind analyses at 1000 mb, energy variables at this level are obtained by linear extrapolation. If the vertical distribution of energy variables in previous studies (e.g., Kung, 1966) is typical, this is a good approximation. Energy variables are assumed to be zero at $p=0$; the trapezoidal rule is used in all vertical integrations. Finally, the dissipation term is evaluated as a residual (Kung, 1966). Holopainen (1973) warns of the risk in attaching physical significance to the sign or magnitude of residual terms, but he concedes that application of the residual technique may be meaningful in data-rich areas where the instruments are accurate and of uniform design. The U. S. radiosonde network that provided data for this study meets these criteria.

4. Synoptic analysis

Figs. 2, 4 and 5 show surface, 500 and 200 mb charts at 1200 GMT on each day from 13 to 15 March 1973. The calculations discussed here cover 72 h, from 0000 GMT 13 March to 0000 GMT 16 March 1973. During this time, a large cyclone originated in the southwestern United States and moved toward the Great Lakes (Fig. 2). Since cyclogenesis occurred entirely within a data-rich area, we are confident in the synoptic-scale analysis of this event. In Fig. 3 the solid line shows the cyclone central pressure as a function of time. Cyclogenesis is already occurring at 0000 GMT 13 March over New Mexico and becomes particularly rapid between 1200 GMT 13 March and 0000 GMT 14 March; the occlusion process begins as the sea-level pressure reaches a minimum of 972 mb. In the next 12 h, the storm fills rapidly as it approaches the Great Lakes. Thereafter, it fills more slowly until leaving the computational area at 0000 GMT 16 March. We regard 0000 GMT 13 March to 1200 GMT 14 March as the growth period and the remaining part of the life cycle as the decay period.

Evolution of the 500 mb cutoff low is shown in Fig. 4. Prior to the time of the first map, a cutoff low is centered over southern California. In response to a short-wave trough moving southeastward into the Pacific North-

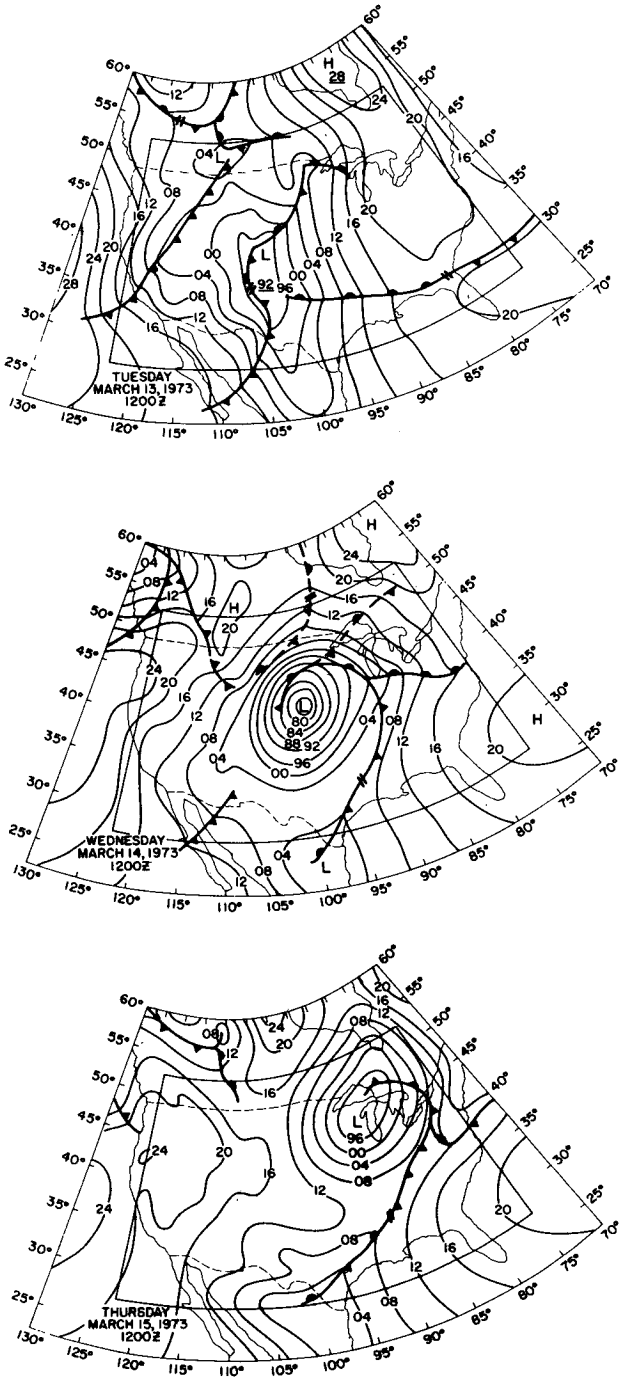

FIG. 2. Analyses of fronts and sea-level pressure at 24 h intervals. Contour interval is 4 mb.

west states, the cutoff low opens into a vigorous and rapidly moving short wave shown at 1200 GMT 13 March over the Great Basin. Just 24 h later, this short wave has developed closed contours over Nebraska, while the second trough settles into the desert southwest states. 500 mb heights have fallen by as much as 300 m in parts of Kansas and Nebraska simultaneously with the deepening of the surface cyclone. By 1200 GMT 14 March, the centers of the surface and 500 mb circulations coincide, signaling that the occlusion process is well under way. During the final 24 h, the southern short wave progresses eastward to the Arizona-New Mexico border. The northern storm weakens considerably; all that remains by 1200 GMT 15 March is a rapidly moving short wave over the upper Great Lakes.

An interesting feature of the 500 mb flow is the change in tilt of the trough axis from northwest–southeast in the growth stage to northeast–southwest in the decay stage. This phenomenon is common in rotating annulus experiments (Hide, 1958; Fultz *et al.*, 1959; Pfeffer and Chiang, 1967). Called the "tilted trough vacillation," it is accompanied by a change in sign of the eddy flux of angular momentum and by fluctuations in magnitude and sign of the conversion rate between zonal and eddy kinetic energy.

The 200 mb flow shown in Fig. 5 is similar to the 500 mb flow, except that the two interacting troughs are less easily distinguished. Noteworthy is the strong jet entering the region from the southwest and leaving it at lesser speed off the New England coast. This situation persists during the three days under study, although on the last day the jet strengthens over New England as the short wave associated with a much weakened Great Lakes "low" begins to move across the long-wave ridge.

5. Kinetic energy budget for the cyclone

a. Time evolution of the kinetic energy budget

We compute the energy budget from terms in the Eulerian kinetic energy equation in a domain which encloses the cyclone during its life cycle. The area-mean energy variables, integrated from 1000 mb to the top of the atmosphere for each synoptic time, are shown in Table 1. The kinetic energy K increases during the growth period, reaches a maximum at 1200 GMT

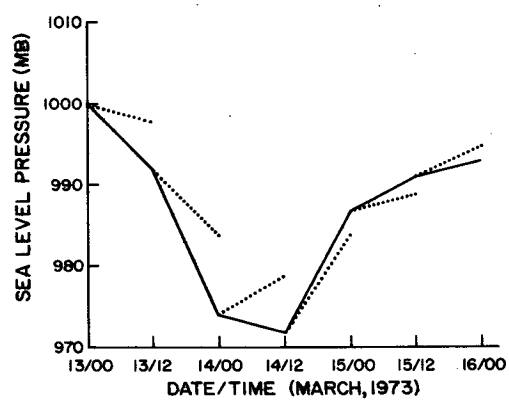

FIG. 3. Observed (solid line) and predicted (dashed line) variation of sea-level pressure at the center of the cyclone. Predicted values are derived from 12 h forecasts by the limited-area, fine-mesh model at the National Meteorological Center.

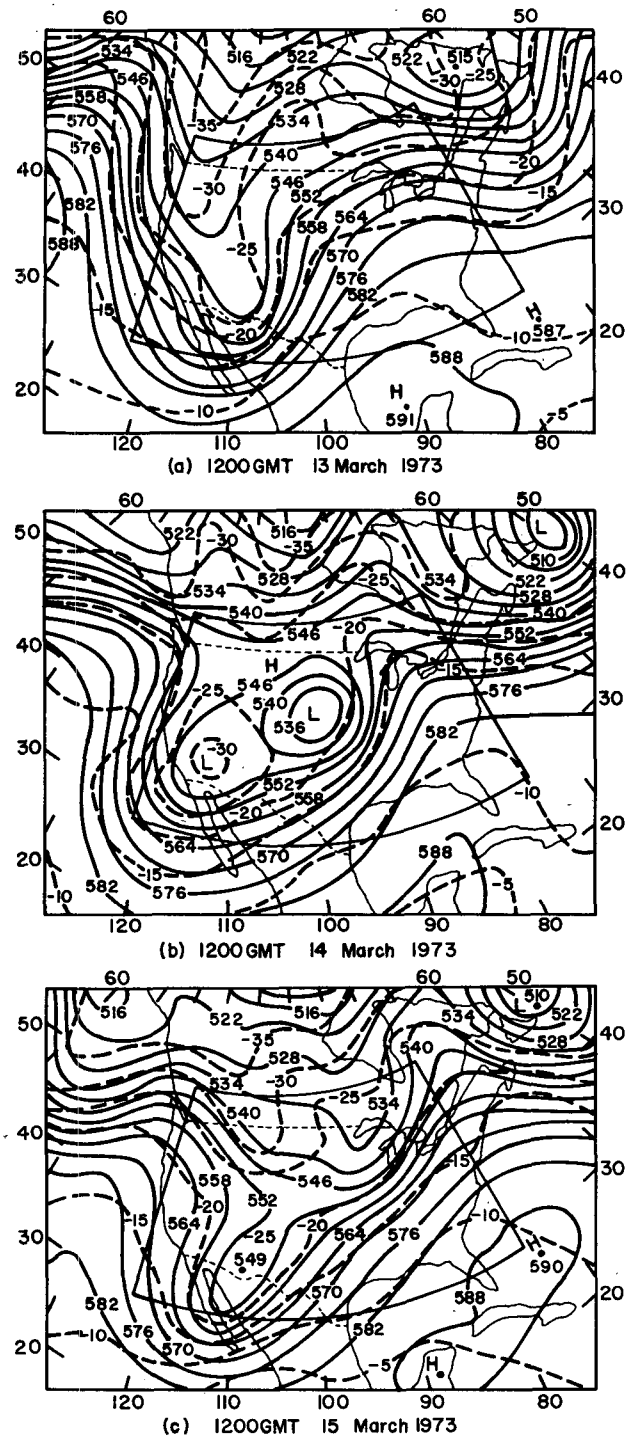

FIG. 4. Contours of height (dam) and temperature (°C) on the 500 mb pressure surface at 24 h intervals.

14 March, and decreases thereafter. The time derivative of kinetic energy, $\partial K/\partial t$, positive during the growth stage and negative during the decay stage, is small compared to K, reflecting the persistence of the upper tropospheric jet during the life of the cyclone.

The horizontal flux convergence of kinetic energy, $-\nabla\cdot(V\dot{k})$, contributes kinetic energy at every analysis time because the inflow jet is stronger than the outflow jet (see Section 4). The gradual strengthening of the outflow jet in the northeast corner of the domain seems to explain the monotonic decrease in horizontal flux

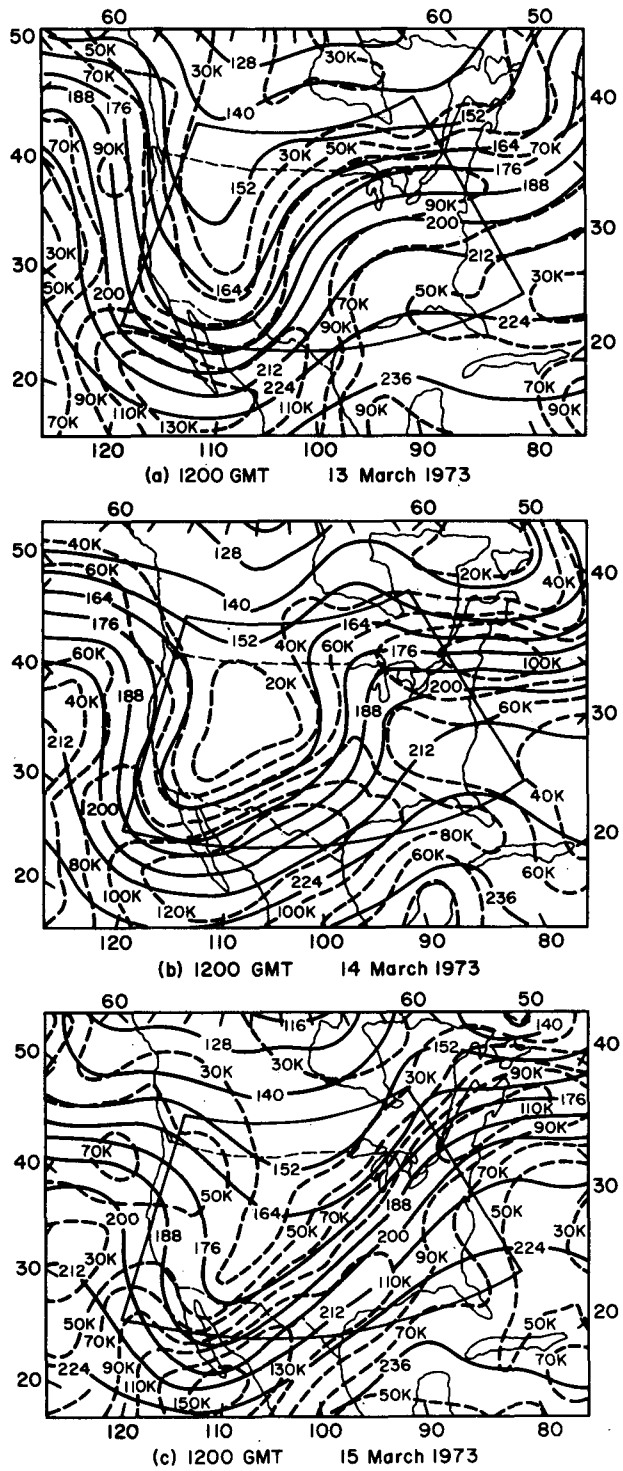

FIG. 5. Contours of height (dam with leading 1 omitted) and isotachs (kt) on the 200 mb pressure surface at 24 h intervals.

TABLE 1. Kinetic energy budget for the storm (1000 mb to the top of the atmosphere). Units: kinetic energy in 10^5 J m^{-2}; kinetic energy changes in W m^{-2}. $\partial K/\partial t$ is calculated from $u(\partial u/\partial t)+v(\partial v/\partial t)$.

	Date/Time	K	$\partial K/\partial t$	$-\nabla\cdot\mathbf{V}k$	$-\mathbf{V}\cdot\nabla\phi$	$D(k)$	$-\mathbf{V}\cdot\nabla\phi-D$
Growth	13/00	28.0	1.9	36.1	−7.9	26.2	−34.1
	13/12	30.4	6.6	40.4	−12.2	21.6	−33.8
	14/00	33.1	4.6	27.2	5.8	28.4	−22.6
	14/12	36.4	1.5	26.8	12.4	37.7	−25.3
Decay	15/00	33.8	−1.7	23.7	5.7	31.1	−25.4
	15/12	31.8	−5.5	20.7	2.7	28.9	−26.2
	16/00	29.1	−5.2	9.4	3.7	18.2	−14.5

convergence after 1200 GMT 13 March. Nevertheless, $-\nabla\cdot(\mathbf{V}k)$ is the major source of kinetic energy for the cyclone.

The generation of kinetic energy is caused by cross-contour flow. Initially this quantity is negative. Examination of geostrophic and ageostrophic winds at 1200 GMT 13 March (maps not shown) reveals super-geostrophic flow across contours toward higher pressure in the ridge over the eastern United States (Figs. 4a and 5a). The major energy *source* in the formative stages of the cyclone is clearly the flux of kinetic energy into the region. At 1200 GMT 14 March, the flow is markedly subgeostrophic around the long-wave trough over the plateau and Rocky Mountain states (Figs. 4b and 5b). The cyclone is at maximum intensity. The predominance of cross-contour flow toward lower pressure, evident in Table 1, is not so obvious to the eye; that is, it is not strongly localized or confined to specific levels.

As expected, the dissipation $D(k)$ is greatest when the storm is most intense.

An overview of the kinetic energy budget is obtained by comparing the external source or sink $-\nabla\cdot(\mathbf{V}k)$ and the internal source or sink $-\mathbf{V}\cdot\nabla\phi-D(k)$ as defined by Smith (1973). Table 1 shows clearly that the external source dominates during the growth stage, but that the reverse is true during the decay stage, when dissipation outweighs positive contributions from net kinetic energy import and cross-isobaric flow toward lower pressure.

b. Vertical distribution of time-mean kinetic budget

The time-mean kinetic energy budget for the storm as a function of pressure is shown in Table 2. The major contribution to kinetic energy comes from a persistent upper tropospheric jet stream. The quantity $-\partial(\omega k)/\partial p$ indicates downward transport of kinetic energy from the jet stream level near 250 mb to the boundary layer, where surface friction removes kinetic energy. The transport mechanism is vertically moving eddies in a positively sheared environment. The generation of kinetic energy $-\mathbf{V}\cdot\nabla\phi$ is negative above the 500 mb level but positive below. Our vertical distribution of $-\mathbf{V}\cdot\nabla\phi$ conflicts with Kung's (1966), in which two positive maxima appear (one each in the upper and lower troposphere), but his result is an average of multi-year data, whereas ours pertains to a particular case. The dissipation of kinetic energy is greatest near the level of maximum wind, where large vertical shear and turbulence might be expected. $D(k)$ also tends to increase near the surface.

It is interesting that different physical processes determine the kinetic energy balance at different levels. Above 200 mb, $-\nabla\cdot(\mathbf{V}k)>-\mathbf{V}\cdot\nabla\phi-D(k)$; that is, horizontal import of kinetic energy more than balances the losses due to cross-contour flow and dissipation. Most of the excess of $-\nabla\cdot(\mathbf{V}k)$ over $-\mathbf{V}\cdot\nabla\phi-D(k)$ is transported downward. Between 250 and 500 mb, the major source is still net horizontal influx of kinetic energy, but $-\nabla\cdot(\mathbf{V}k)$ is slightly smaller than $-\mathbf{V}\cdot\nabla\phi$

TABLE 2. Time-mean kinetic energy budget for the storm as a function of pressure. Units: kinetic energy in kJ m^{-2} kPa^{-1}; kinetic energy changes in 10^{-5} W m^{-2} kPa^{-1}. Vertical integrals of energy variables have same units as in Table 1.

Pressure	k	$\partial k/\partial t$	$-\nabla\cdot(\mathbf{V}k)$	$-\partial(\omega k)/\partial p$	$-\mathbf{V}\cdot\nabla\phi$	$D(k)$	$-\mathbf{V}\cdot\nabla\phi-D(k)$
150	51.3	0.7	58.3	−16.2	−22.4	19.0	−41.4
200	73.6	1.6	101.2	−14.4	−46.8	38.3	−85.1
250	83.0	−3.9	115.1	5.8	−8.7	116.1	−124.8
300	73.0	−0.2	68.6	12.0	−15.2	65.6	−80.8
400	48.1	0.6	34.9	3.1	−2.5	34.9	−37.4
500	31.1	−0.9	3.3	1.5	−2.0	3.7	−5.7
700	12.9	−0.2	2.0	1.8	7.6	11.6	−4.0
850	7.8	0.2	1.4	1.0	19.8	22.0	−2.2
1000	2.7	0.6	0.8	0.2	32.0	32.4	−0.4
Vertical integral	31.8	−0.2	26.3	0.0	1.4	27.8	−26.4

TABLE 3. Comparison of kinetic energy budgets for different storms. Units same as in Table 1. CAS (present study) 1000 mb to the top of the atmosphere; S (Smith, 1973) surface to 200 mb; PS (Petterssen and Smebye, 1971), surface to 100 mb.

Study	K	$\partial K/\partial t$	$-\nabla\cdot(\mathbf{V}k)$	$-\partial(\omega k)/\partial p$	$-\mathbf{V}\cdot\nabla\phi$	$D(k)$	$-\mathbf{V}\cdot\nabla\phi-D(k)$
Growth period							
CAS	32.0	3.7	32.6	0.0	−0.5	28.5	−29.0
S	19.2	6.5	12.0	0.0	10.0	15.5	−5.5
PS	27.2	2.8	−9.7	−1.0	19.8	6.3	13.5
Decay period							
CAS	31.6	−4.1	17.9	0.0	4.0	26.0	−22.0
S	19.0	−3.8	9.5	0.0	0.1	13.4	−13.3
PS	26.3	−2.8	−9.4	−1.0	16.0	8.4	7.6

$-D(k)$. Below 500 mb, the generation of kinetic energy $-\mathbf{V}\cdot\nabla\phi$ is the major energy source; $-\nabla\cdot(\mathbf{V}k)$ contributions are small. Taken together, these two sources do not offset the dissipation. The deficit of kinetic energy near the surface is caused by frictional drag and induces a downward transport from above.

c. *Comparison with previous studies*

Three different case studies are compared briefly: Petterssen and Smebye (1971), Smith (1973), and the present one (hereafter identified by PS, S, and CAS, respectively. We rely on Smith's (1973) discussion of PS's results as well as his own. Table 3 summarizes our comparisons.

The development of surface cyclones is similar in all three cases, but there are differences in the upper air circulation. In PS, the major jet stream leaves the cyclogenetic region over the Atlantic Ocean. In S, a persistent jet stream enters the region from the west and northwest. The upper air circulation in CAS is similar to that in S, except that the jet stream is stronger and the 500 mb cutoff low is more pronounced.

Very different processes are responsible for the major sources and sinks. During the growth stage in CAS, the net horizontal transport of kinetic energy into the region by the jet stream is the principal energy source. In S the import of kinetic energy by the jet stream and the generation of kinetic energy by the cross-contour flow are equally important sources. In PS, however, the kinetic energy generated by cross-contour flow is exported from the storm area by the existing jet stream. During the decay stage, both CAS and S show horizontal influx of kinetic energy by the jet stream, which slows the decline of the storm, but PS maintains the same situation that occurred during the growth stage.

The comparison between CAS and S suggests that the intrusion of a jet stream into the storm area can supply much of the kinetic energy for development.

6. Contribution of divergent and nondivergent wind components to the kinetic energy budget for the cyclone

a. *Kinetic energy*

In their global study, Chen and Wiin-Nielsen (1976) showed that the kinetic energy K_D of the divergent wind is very small compared to that of the nondivergent wind K_R. However, Chen (1975) noted that K_D may be significant in severe storms. In Table 4 we show the contribution of the divergent wind to the kinetic energy of the cyclone of 13–16 March 1973 and the ratios K_R/K, K_D/K, and $\mathbf{V}_R\cdot\mathbf{V}_D/K$ at 12 h intervals during cyclone evolution. K, K_R and K_D all vary in the same direction except that K_D increases in the last 12 h while K and K_R decrease. The dot product of the nondivergent and divergent winds $\mathbf{V}_R\cdot\mathbf{V}_D$ integrates to zero on the globe, but not necessarily in a limited-area domain. In our case $\mathbf{V}_R\cdot\mathbf{V}_D$ is smaller than K_D.

TABLE 4. Kinetic energies K, K_R, K_D, and $\mathbf{V}_R\cdot\mathbf{V}_D$ and the ratios K_R/K, K_D/K and $\mathbf{V}_R\cdot\mathbf{V}_D/K$ for the storm. Units: kinetic energy in 10^5 J m^{-2}.

Date/Time		K	K_R	K_D	$\mathbf{V}_R\cdot\mathbf{V}_D$	K_R/K	K_D/K	$\mathbf{V}_R\cdot\mathbf{V}_D/K$
Growth	13/00	28.0	27.7	0.42	−0.09	98.8%	1.5%	−0.3%
	13/12	30.4	30.1	0.52	−0.22	99.0%	1.7%	−0.7%
	14/00	33.1	32.6	0.85	−0.34	98.5%	2.6%	−1.1%
	14/12	36.4	36.1	0.90	−0.61	99.2%	2.5%	−1.7%
Decay	15/00	33.8	33.6	0.87	−0.59	99.2%	2.6%	−1.8%
	15/12	31.8	31.7	0.84	−0.74	99.7%	2.6%	−2.3%
	16/00	29.1	28.1	0.91	0.10	96.5%	3.1%	0.4%
Time average		31.8	31.4	0.76	−0.36	98.7%	2.4%	−1.1%

TABLE 5. Kinetic energies K, K_R, K_D and $\mathbf{V}_R \cdot \mathbf{V}_D$ for the storm as a function of pressure. Units: kJ m^{-2} kPa^{-1}.

Pressure	K	K_R	K_D	$\mathbf{V}_R \cdot \mathbf{V}_D$
150	51.3	51.3	0.88	−0.87
200	73.6	73.7	1.45	−1.57
250	83.0	83.2	1.52	−1.67
300	73.0	73.3	1.36	−1.69
400	48.1	48.4	0.66	−1.03
500	31.1	30.6	0.45	0.10
700	12.9	12.3	0.42	0.16
850	7.8	7.2	0.52	0.05
1000	2.8	2.1	0.62	−0.06

The error in approximating K by K_R ranges from 1 to 4%; the average error during the 3-day period is only 1.3%.

In Table 5 the total kinetic energy is partitioned by pressure level. K is slightly less than K_R at 400 mb and above, but slightly greater below, in accordance with the sign of $\mathbf{V}_R \cdot \mathbf{V}_D$—negative at 400 mb and above and positive below. The level of maximum K and K_R (250 mb) coincides with the level of maximum wind. The variation of K_D with pressure is similar to that observed in a global case studied by Chen and Wiin-Nielsen (1976); that is, K_D attains its peak value at the jet stream level.

We have also examined vector plots of $\mathbf{V}_R$ and $\mathbf{V}_D$ (not shown). In the lower troposphere, the divergent wind generally flows across the streamlines toward lower pressure. Since the angle between the nondivergent and divergent wind directions is large, $\mathbf{V}_R \cdot \mathbf{V}_D$ is small. In the upper troposphere these wind directions tend to be opposed; hence, $\mathbf{V}_R \cdot \mathbf{V}_D$ is larger and negative there.

b. *Horizontal flux convergence of kinetic energy*

The horizontal flux convergence of kinetic energy is regarded as an external energy source and represents the net flow into or out of the open system. The total flux convergence of kinetic energy, $-\nabla \cdot (\mathbf{V}k)$, is split into two parts, one due to the nondivergent wind $-\nabla \cdot (\mathbf{V}_R k)$ and the other to the divergent wind $-\nabla \cdot (\mathbf{V}_D k)$. These quantities and the ratios of each part to the total are shown in Table 6.

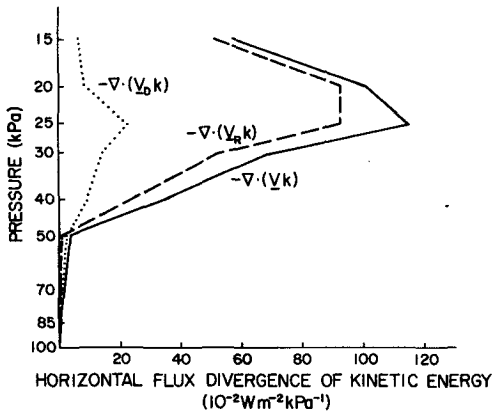

FIG. 6. Time-averaged kinetic energy flux divergence of the total wind (solid line), the nondivergent wind (dashed line) and the divergent wind (dotted line).

We have shown that K_D is two orders of magnitude less than K_R; yet during the last 24 h of the decay stage, the divergent component of the wind contributes one-quarter to one-half the total flux convergence of kinetic energy. $-\nabla \cdot (\mathbf{V}_R k)$ decreases steadily as $-\nabla \cdot (\mathbf{V}k)$ does, and becomes small at 0000 GMT 16 March. By contrast, the horizontal flux convergence of kinetic energy due to the divergent part of the wind $-\nabla \cdot (\mathbf{V}_D k)$ is initially small but increases to a maximum during the mature stage. The time-mean $-\nabla \cdot (\mathbf{V}_D k)$ is roughly one-quarter of the time-mean of $-\nabla \cdot (\mathbf{V}_R k)$. Neglecting the divergent part of the wind in this case would clearly lead to sizable errors in the calculation of $-\nabla \cdot (\mathbf{V}k)$.

Fig. 6 shows the pressure variation of horizontal flux convergence terms. $-\nabla \cdot (\mathbf{V}_R k)$ is much greater than $-\nabla \cdot (\mathbf{V}_D k)$ above 400 mb but smaller below. The largest values of $-\nabla \cdot (\mathbf{V}_D k)$ occur in the upper troposphere, where both $\mathbf{V}_R$ and $\mathbf{V}_D$, are strongest.

TABLE 6. Horizontal flux converges of kinetic energy by total wind $[-\nabla \cdot (\mathbf{V}k)]$, by nondivergent wind $[-\nabla \cdot (\mathbf{V}_R k)]$ and by divergent wind $[-\nabla \cdot (\mathbf{V}_D k)]$, and the ratios $-\nabla \cdot (\mathbf{V}_R k)/-\nabla \cdot (\mathbf{V}k)$ and $-\nabla \cdot (\mathbf{V}_D k)/-\nabla \cdot (\mathbf{V}k)$. Units: horizontal flux convergence of kinetic energy in W m^{-2}.

	Date/Time	$-\nabla \cdot (\mathbf{V}k)$	$-\nabla \cdot (\mathbf{V}_R k)$	$-\nabla \cdot (\mathbf{V}_D k)$	$-\nabla \cdot (\mathbf{V}_R k)/-\nabla \cdot (\mathbf{V}k)$	$-\nabla \cdot (\mathbf{V}_D k)/-\nabla \cdot (\mathbf{V}k)$
Growth	13/00	36.1	31.9	4.2	88.4%	11.6%
	13/12	40.4	36.1	4.3	89.4%	10.6%
	14/00	27.2	24.1	3.1	88.6%	11.4%
	14/12	26.8	20.0	6.8	74.6%	25.4%
Decay	15/00	23.7	16.5	7.2	69.6%	30.4%
	15/12	20.7	15.9	4.8	76.8%	23.2%
	16/00	9.4	4.7	4.7	50.0%	50.0%
Time average		26.3	21.3	5.0	76.8%	23.2%

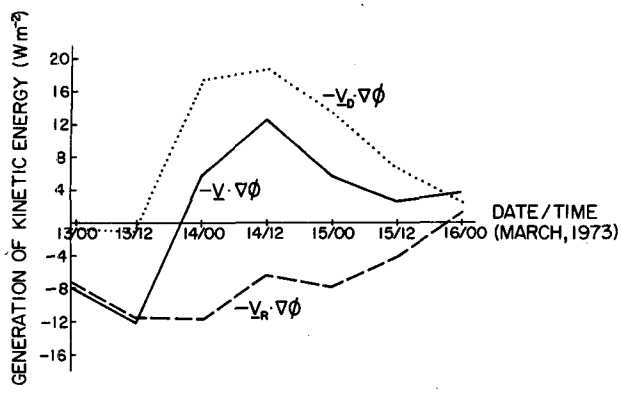

FIG. 7. Vertically averaged kinetic energy generation by the total wind (solid line), the nondivergent wind (dashed line) and the divergent wind (dotted line).

c. Generation of kinetic energy

Past studies of cyclogenesis show that development may be initiated by baroclinic instability (Eady, 1949; Charney, 1947), by amplification of barotropic waves (Kuo, 1949), or by a combination of both (Pedlosky, 1964a,b). To broaden our knowledge of the energetics of cyclogenesis, we now compare this observational study with others reported in the literature. We discuss the partitioning of kinetic energy generation into baroclinic and barotropic parts as in Eq. (6).

The generation of kinetic energy at different times in the life of the cyclone is shown in Fig. 7. The barotropic contribution $-\mathbf{V}_R\cdot\nabla\phi$ is negative except at 0000 GMT 16 March; that is, the nondivergent wind blows toward higher pressure most of the time. The baroclinic contribution $-\mathbf{V}_D\cdot\nabla\phi$ behaves differently. Early in the development stage, $-\mathbf{V}_D\cdot\nabla\phi$ is small and negative. Later, as the cyclone matures, $-\mathbf{V}_D\cdot\nabla\phi$ becomes large, reaching its maximum value when the cyclone is most intense. After 0000 GMT 14 March, $-\mathbf{V}_D\cdot\nabla\phi$ is the dominant term. Evidently, the baroclinic term contributes toward kinetic energy generation whereas the barotropic term contributes negatively, i.e., tends to convert kinetic energy to available potential energy. The cross-contour flow due to the divergent wind is predominantly toward lower pressure. During the first 24 h of cutoff development, it is likely that the centrifugal force is greater than the sum of the pressure gradient and Coriolis forces, and thus the divergent flow is channeled toward higher pressure. At any rate, barotropic and baroclinic processes are opposed, resulting in little generation of kinetic energy.

In Section 2, we mentioned that the integral of $-\mathbf{V}_R\cdot\nabla\phi$ over the whole globe is zero. Presumably, mass exchange between the two hemispheres is unimportant. Although we claim that the major energy source for this storm is the horizontal flux divergence of kinetic energy, this quantity also integrates to zero over the globe. The main contribution of an open system to global (or hemispheric) energetics, therefore, comes from the baroclinic generation of kinetic energy. The positive value of $-\mathbf{V}_D\cdot\nabla\phi$ indicates that this cyclone contributes toward the global conversion of available potential energy to kinetic energy.

Generation of kinetic energy as a function of pressure is shown in Fig. 8. Generation due to barotropic processes predominates at 500 mb and above and is negative, whereas generation due to baroclinic processes is positive, except above 200 mb. In his study of a developing baroclinic wave, Krishnamurti (1968) found that upper tropospheric cross-contour flow over large areas could be explained by nondivergent wind components. He also observed that the nondivergent wind blows toward higher pressure in the northwesterly current to the rear of the trough and toward lower pressure in the southwesterly flow ahead of it. This implies that $-\mathbf{V}_R\cdot\nabla\phi$ is negative west of the trough and positive east of it. The negative value of the area-mean of $-\mathbf{V}_R\cdot\nabla\phi$ in Fig. 8 is most likely caused by an imbalance between values of $-\mathbf{V}_R\cdot\nabla\phi$ on opposite sides of the trough. Hsieh's (1949) detailed analysis of cutoff lows mentions asymmetric isotach patterns around a trough with stronger northwesterly winds frequently appearing to the west of the trough during cutoff development. The cutoff low decays as the wind field becomes more symmetric about the trough line. The conclusions of Krishnamurti and of Hsieh explain the occurrence of negative values of $-\mathbf{V}_R\cdot\nabla\phi$ in the upper troposphere of the present study and the approach toward positive values as the storm decays. Both $-\mathbf{V}_R\cdot\nabla\phi$ and $-\mathbf{V}_D\cdot\nabla\phi$ are positive below 500 mb, implying that both divergent and nondivergent winds flow across contours toward lower pressure.

d. Kinetic energy budget for a storm without divergent wind

We have just examined the contribution of the divergent and nondivergent winds to the kinetic energy

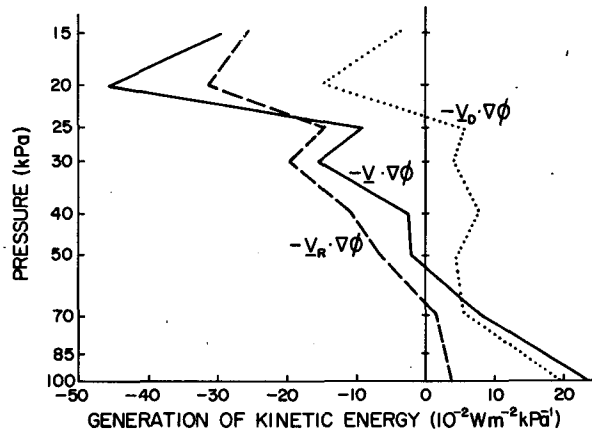

FIG. 8. Time-averaged generation of kinetic energy by the total wind (solid line), the nondivergent wind (dashed line) and the divergent wind (dotted line).

budget of the storm. In this subsection we show how neglect of the divergent wind affects the kinetic energy budget.

According to Chen and Wiin-Nielsen's (1976) computations with data from the National Center for Atmospheric Research (NCAR) general circulation model (Kasahara and Washington, 1971), the divergent wind contributes about one-tenth of the total dissipation. Furthermore, neglect of the divergent wind causes about a 1% error in the calculation of total kinetic energy of the cyclone and, consequently, very slight errors in the calculation of $-\nabla\cdot(\mathbf{V}_R k)$. We ignore this error in the following discussion.

Table 7 shows the kinetic energy budget for each synoptic time. Primes indicate neglect of the divergent wind. $\partial K'/\partial t$ is evaluated from (8) as a residual. $\partial K/\partial t - \partial K'/\partial t$ is regarded as the deficit in the rate at which energy is supplied to the cyclone as a result of neglecting the divergent wind. $\partial K/\partial t - \partial K'/\partial t$ increases during the growth state and decreases during the decay stage. The divergent wind is obviously very important during the mature stage of the storm, from 0000 GMT 14 March to 0000 GMT 15 March. In fact, the cyclone would fill rather than deepen from 0000 to 1200 GMT on 14 March and fill more rapidly in the next 12 h if the divergent wind component were neglected.

Numerical prediction models generally utilize smoothed or filtered fields in order to prevent the spurious effects often induced by gravity waves. The above discussion suggests that if smoothing or filtering removes part or all of the divergence from the initial wind field, the forecast may contain significant errors from the start.

A recent paper by Dey and McPherson (1977) indicates that divergent initialization neither degrades nor improves the performance of the *global* analysis/forecast system now operational at the National Meteorological Center (NMC). The authors emphasize, however, that this conclusion may not apply to fine mesh models and suggest further research in this area. Fig. 3 compares the observed central pressure with 12 h predicted values from the limited-area, fine-mesh (LFM) model at NMC. The rates of deepening and filling are both underforecast by the LFM. We cannot expect any model to make perfect 12 h forecasts, but the nature of this error and our conclusions about the importance of the divergent wind suggest an interesting experiment: run two 12 h forecasts, one with the divergent component included in the initial wind field, the other with the divergent component removed. If the problem of noise could be overcome, such an experiment might indicate the advantage, if any, of including the divergent wind in the initial conditions.

TABLE 7. Kinetic energy budget for the storm (1000 mb to the top of the atmosphere), neglecting the contribution of the divergent wind component. Units: W m^{-2}.

Date/ Time	$\partial K/\partial t - \partial K'/\partial t$	$\partial K'/\partial t$	$-\nabla\cdot(\mathbf{V}_R k)$	$-\mathbf{V}_R\cdot\nabla\phi$	90% $D(k)$
13/00	0.8	1.1	31.9	−7.2	23.6
13/12	1.2	5.4	36.1	−11.3	19.4
14/00	17.6	−13.1	24.1	−11.5	25.7
14/12	21.7	−20.2	20.0	−6.3	33.9
15/00	17.6	−19.3	16.5	−7.8	28.0
15/12	8.6	−14.1	15.9	−4.0	26.0
16/00	5.2	−10.4	4.7	1.3	16.4

7. Summary and remarks

We have studied a short-wave disturbance (13–16 March 1973) which evolved into a cutoff low aloft and spawned an intense surface cyclone. Import of kinetic energy by a strong and persistent jet stream in the upper troposphere provided most of the energy for development. The generation of kinetic energy by cross-contour flow was a secondary energy source. These results differ significantly from those of previous studies.

We have considered the separate contributions to the kinetic energy budget by divergent and nondivergent winds (denoted by $\mathbf{V}_D$ and $\mathbf{V}_R$, respectively). We find that $\mathbf{V}_D$ contributes 1–2% of the total kinetic energy but nearly 25% of the flux convergence of total kinetic energy during the lifetime of the storm. The generation of kinetic energy by baroclinic processes, $-\mathbf{V}_D\cdot\nabla\phi$, is 8.1 W m^{-2} and that by barotropic processes, $-\mathbf{V}_R\cdot\nabla\phi$, is −6.4 W m^{-2} averaged over the lifetime of the storm (ϕ is geopotential).

When calculating the magnitude of kinetic energy, one may safely replace the total wind with the nondivergent wind. But the horizontal flux convergence of kinetic energy and the generation of kinetic energy are sensitive to the magnitude of the divergent wind. Any significant reduction of the divergent wind component effected by smoothing or filtering analyzed wind fields would result in sizable errors in the time variation of kinetic energy of this storm.

The treatment of initial data has long been a vexing problem in primitive equation prediction models. To avoid the generation of gravity waves which could mask the evolution of synoptic-scale waves with small-scale "noise," meteorologists have designed schemes to reduce or remove the divergent wind component. Our results suggest, however, that significant modification of $\mathbf{V}_D$ in the initial wind field could change the evolution of the numerical forecast in cases of cyclogenesis.

Acknowledgments. This investigation, conducted jointly by the National Center for Atmospheric Research and the University of Michigan, was initiated while Tsing-Chang Chen was affiliated with the University of Michigan. Chen was partially supported by NASA under Contract NSG-2010 and Alpert by NSF Grant ATM 76-82569. We appreciate the en-

couragement and help of Professors Aksel Wiin-Nielsen and Ferdinand Baer, and we acknowledge Mr. Grant Branstator's assistance in preparing the data and running the limited-area objective analysis program. Cheryl Pierce typed the first draft; Ann Modahl and Lois Gries typed and edited subsequent drafts.

REFERENCES

Charney, J. G., 1947: The dynamics of long waves in a baroclinic westerly current. *J. Meteor.*, **4**, 135–162.

——, 1955: The use of the primitive equation of motion in numerical prediction. *Tellus*, **7**, 22–26.

——, R. Fjørtoft and J. von Neumann, 1950: Numerical integration of the barotropic vorticity equation. *Tellus*, **2**, 237–254.

Chen, T.-C., 1975: On the kinetic energy of the divergent and nondivergent flow in the atmosphere. Tech. Rep. 002630-14-T, Dept. Atmos. Oceanic Sci., University of Michigan, 143 pp.

——, and A. Wiin-Nielsen, 1976: On the kinetic energy of the divergent and nondivergent flow in the atmosphere. *Tellus*, **28**, 486–498.

Dey, C. H., and R. D. McPherson, 1977: An experiment in global divergent initialization. *Mon. Wea. Rev.*, **105**, 1372–1383.

Eady, E. T., 1949: Long waves and cyclone waves. *Tellus*, **1**, 33–52.

Endlich, R. M., 1967: An iterative method for altering the kinetic properties of wind fields. *J. Appl. Meteor.*, **6**, 837–844.

Fultz, D., R. Long, G. Owens, W. Bohan, R. Kaylor and J. Weil, 1959: Studies of thermal convection in a rotating cylinder with some implications for large-scale atmospheric motions. *Meteor. Monogr.*, No. 21, 1–104.

Gandin, L. S., 1963: *Objective Analysis of Meteorological Fields*. Gidrometeor., Leningrad. [Israel Program for Scientific Translations, 1965, 242 pp.]

Haltiner, G. J., 1971: *Numerical Weather Prediction*. Wiley, 317 pp.

——, and F. L. Martin, 1957: *Dynamical and Physical Meteorology*. McGraw-Hill, 470 pp. (see pp. 322–329).

Hide, R., 1958: An experiment on thermal convection in a rotating fluid. *Phil. Trans. Roy. Soc. London*, **A250**, 441–478.

Holopainen, E., 1973: An attempt to determine the effects of turbulent friction in the upper troposphere from the balance requirements of the large-scale flow: A frustrating experiment. *Geophysica*, **12**, 151–176.

Hsieh, Y.-P., 1949: An investigation of a selected cold vortex over North America. *J. Meteor.*, **6**, 401–410.

Kasahara, A., and W. Washington, 1971: General circulation experiments with a six-layer NCAR model, including orography, cloudiness, and surface temperature calculations. *J. Atmos. Sci.*, **28**, 657–701.

Krishnamurti, T. N., 1968: A study of a developing wave cyclone. *Mon. Wea. Rev.*, **96**, 208–217.

Kung, E. C., 1966: Kinetic energy generation and dissipation in the large-scale atmospheric circulation. *Mon. Wea. Rev.*, **94**, 67–82.

Kuo, H.-L., 1949: Dynamic instability of two-dimensional nondivergent flow in a barotropic atmosphere. *J. Meteor.*, **6**, 278–295.

O'Brien, J. J., 1970: Alternative solutions to the classical vertical velocity problem. *J. Appl. Meteor.*, **9**, 197–203.

Pearce, R. P., 1974: The design and interpretation of diagnostic studies of synoptic-scale atmospheric systems. *Quart. J. Roy. Meteor. Soc.*, **100**, 265–285.

Pedlosky, J., 1964a: The stability of currents in the atmosphere and the ocean, Part I. *J. Atmos. Sci.*, **21**, 201–219.

——, 1964b: The stability of currents in the atmosphere and the ocean, Part II. *J. Atmos. Sci.*, **21**, 342–353.

Petterssen, S., and S. J. Smebye, 1971: On the development of extratropical cyclones. *Quart. J. Roy. Meteor. Soc.*, **7**, 457–482.

Pfeffer, R. L., and Y. Chiang, 1967: Two kinds of vacillation in rotating laboratory experiments. *Mon. Wea. Rev.*, **95**, 75–82.

Richardson, L. F., 1922: *Weather Prediction by Numerical Process*. Cambridge University Press, 236 pp.

Schlatter, T. W., 1975: Some experiments with a multivariate statistical objective analysis scheme. *Mon. Wea. Rev.*, **103**, 246–257.

——, G. W. Branstator and L. G. Thiel, 1976: Testing a global multivariate statistical objective analysis scheme with observed data. *Mon. Wea. Rev.*, **104**, 765–783.

Smith, P. J., 1973: The kinetic energy budget over North America during a period of major cyclone development. *Tellus*, **25**, 411–423.

Thompson, P. D., 1961: *Numerical Weather Analysis and Prediction*. Macmillan, 170 pp.

Washington, W. M., and D. P. Baumhefner, 1975: A method of removing Lamb waves from initial data for primitive equation models. *J. Appl. Meteor.*, **14**, 114–119.